A Theoretical Study of Sea Surface Up/Down Wind Brightness Temperature Differences

Joel T. Johnson, *Member, IEEE*, and Yongyao Cai

***Abstract*—The small slope approximation (SSA) for polarimetric thermal emission from a rough surface is applied to study the up/down wind difference of sea surface brightness temperatures. A complete third-order theory is used, with results expressed in terms of an integral over the sea surface bispectrum. An approximation is developed to obtain emission contributions for surface length scales much larger than the electromagnetic wavelength and in this limit, the up/down wind brightness temperature difference is determined entirely by a combination of third moments of surface slope. Polarization dependencies in this limit however do not match those obtained from the Jet Propulsion Laboratory (JPL) WindRAD empirical model. Another approximation is derived to capture up/down wind emission asymmetry due to short waves which are modulated by longer waves. In this case, an integral of emission "weighting functions" over a pair of "reduced" bispectra is obtained, and examination of the weighting functions shows the importance of surface length scales comparable to the electromagnetic wavelength. The polarization dependencies of these weighting functions illustrate the possibility of matching the WindRAD model, but the absence of an effective hydrodynamic model for short gravity-capillary wave modulation by longer waves limits detailed comparisons.**

***Index Terms*—Microwave radiometry, ocean remote sensing, rough surface scattering, thermal emission.**

I. Introduction

RECENT experimental and theoretical studies have demonstrated the utility of polarimetric techniques in microwave passive remote sensing of ocean wind speed and direction [1]–[4]. The success of these studies has resulted in plans for a polarimetric radiometer to be included in the NPOESS series of satellites [5] and for a polarimetric radiometer to orbit as part of the WindSAT program [6]. Analytical and numerical models for the calculation of ocean surface polarimetric thermal emission have also been developed [7]–[10], primarily through application of standard surface scattering approximate methods to calculate surface emissivity using Kirchhoff's law. Models based on both the small perturbation method (SPM) and the physical optics (PO) approximation have been presented, as well as some limited numerical studies of short gravity/capillary wave emission with the method of moments [11]. Reference [10] has further revealed that use of the SPM for emission calculations results in a small slope, rather than small height, emission approximation identical in form to that which would be obtained from the small slope approximation (SSA) of [12], so that the SPM can provide accurate emission predictions even for surfaces with large heights in terms of the electromagnetic wavelength. Numerical tests of the SPM for a set of canonical periodic surfaces have confirmed this statement [13], [14]. These results motivate use of the small slope approximation (SSA) for the study of ocean polarimetric thermal emission since ocean surface slopes are often relatively small on average.

The SSA theory produces a perturbation series in surface slope in which the zeroth-order term reproduces emission from a flat surface, the first-order term identically vanishes, and the second-order term produces the first emission correction due to the presence of surface roughness. This correction is expressed as an integral over the surface directional spectrum weighted by an emission "weighting function" [15]. Previous studies of sea surface emission with the SSA have used the second-order theory [7], [8], [15], [16] with differing models of the sea surface directional spectrum from the literature. However, since the second-order roughness correction involves only the surface directional spectrum, and since the directional spectrum by definition is symmetric under a 180° rotation, it is not possible to obtain an up/down wind brightness difference from the second-order theory. Since up/down wind differences have been clearly observed in measured data [17], improvement on the second-order SSA is necessary to provide agreement with measurements.

This problem has been addressed in [8] through a composite surface emission model, in which the second-order SSA was used to compute emission from individual surface "facets," which were then tilted over a long wave slope distribution. Up/down wind asymmetry was introduced through a long-short wave modulation mechanism, with short wave spectral amplitudes multiplied by an empirical function of long wave slopes. Resulting predictions of up/down wind emission differences showed reasonable agreement with measured data. However, the modulation function used was not directly derived from hydrodynamic considerations, and choice of a "cutoff" parameter was required to separate long and short scales.

A third-order SSA theory would provide more consistent predictions of up/down wind emission differences, since no "cutoff" parameter is directly required and since third-order statistics of a random process (i.e., the bispectrum) can capture surface horizontal asymmetry. However, derivation of the complete third-order expressions is very tedious. Recently, [18] investigated the third-order SSA theory the through use of a tilting approximation for the required third-order kernels,

Manuscript received September 1, 2000; revised September 27, 2001. This work was supported by ONR Contracts N00014-97-1-0541 and N00014-00-1-0399.

The authors are with the Department of Electrical Engineering and ElectroScience Laboratory, The Ohio State University, Columbus, OH 43210 USA (e-mail: johnson@ee.eng.ohio-state.edu).

Publisher Item Identifier S 0196-2892(02)01414-6.

and effects of long wave asymmetry and long–short wave modulation were explored. However, detailed analyses of the model and its results, in particular with respect to polarization dependencies, were not provided.

In this paper, a complete third-order SSA theory is applied to study sea surface up/down wind emission differences through use of the third-order scattering functions derived in [19], [20]. The third-order emission theory is derived and presented in Section II, and resulting brightness temperature contributions are expressed as a fourfold integral over the sea surface bispectrum multiplied by an emission weighting function. Since knowledge of the four-dimensional (4-D) bispectrum of the sea surface is currently very limited (some data for shoaling gravity waves have been obtained in [21]), direct predictions from the third-order theory are not possible at this time. However, approximations can be derived for the long wave asymmetry and long-short wave modulation contributions considered by [18] to provide insight into the emission process. These studies are described in Sections III and IV, respectively. The approximations are applied in a comparison with the JPL WindRad empirical model [17], but as described in [18], the absence at present of an effective model for short gravity-capillary wave modulation by longer waves and wind effects limits the comparisons. A final discussion of the results presented concludes the paper, while properties and models of the surface bispectrum are discussed in Appendices A and B.

Note that the influence of surface foam and atmospheric emission are not considered in this paper, although both can potentially contribute to azimuthal variations of measured brightness temperatures. Reference [9] shows that SSM/I measured up/down wind asymmetries can be approximately predicted through a model which includes only long wave and surface foam asymmetry effects in a Monte Carlo simulation. The results of this paper apply only to emission effects due to the shape of the sea surface.

II. Third-Order SSA Expressions

Polarimetric passive remote sensing involves measurement of all four modified Stokes parameters of the microwave thermal emission

$$\overline{T}_B = \begin{bmatrix} T_{Bh} \\ T_{Bv} \\ T_U \\ T_V \end{bmatrix} = T_s \left(\begin{bmatrix} 1 - r_h \\ 1 - r_v \\ -r_U \\ -r_V \end{bmatrix} \right) \tag{1}$$

where T_{Bh} and T_{Bv} are the brightness temperatures measured by horizontally and vertically polarized antennas, respectively, and T_U and T_V are proportional to the real and imaginary parts of the correlation between fields in horizontal and vertical polarizations, respectively, [7]. The second equality follows from Kirchhoff's Law, which relates the emissivity of a medium at constant temperature to the corresponding reflectivity (r_h, r_v, r_U, and r_V) multiplied with the surface physical temperature T_s (assumed to be 283 K in this paper). Reflectivities are calculated as an integral of bistatic scattering coefficients over the upper hemisphere in the reciprocal active scattering problem [22].

Particular interest in ocean wind remote sensing is given to brightness temperature variations in azimuth, and it is often convenient to represent these variations in terms of a set of azimuthal harmonics. Due to the statistical reflection symmetry of an ocean surface about the wind direction, it can be shown [23] that an appropriate expansion is

$$\begin{bmatrix} T_{Bh} \\ T_{Bv} \\ T_U \\ T_V \end{bmatrix} \approx \begin{bmatrix} T_{Bh}^{(0)} + T_{Bh}^{(1)} \cos\phi_i + T_{Bh}^{(2)} \cos 2\phi_i \\ T_{Bv}^{(0)} + T_{Bv}^{(1)} \cos\phi_i + T_{Bv}^{(2)} \cos 2\phi_i \\ T_U^{(1)} \sin\phi_i + T_U^{(2)} \sin 2\phi_i \\ T_V^{(1)} \sin\phi_i + T_V^{(2)} \sin 2\phi_i \end{bmatrix} \tag{2}$$

where ϕ_i denotes the azimuth angle between the radiometer look direction and wind direction with $\phi_i = 0^\circ$ corresponding to upwind observation. The azimuthal harmonic coefficients $T_\gamma^{(i)}$ for $\gamma = h, v, U,$ or V remain functions of the radiometer polar observation angle θ_i, the frequency of observation f, the relative permittivity of sea water ϵ, and the statistical properties of the surface.

To simplify the calculations, the expressions of this paper describe the difference between brightness temperatures measured in the up and down wind directions. This up/down wind difference directly determines first azimuthal harmonic coefficients $T_\gamma^{(1)}$ in the context of (2), but more accurately is expressed as a summation over all possible odd azimuthal harmonics. Because it is generally expected for moderate slope sea surfaces that the contributions of higher odd harmonics to the up/down wind asymmetry should be relatively weak compared to the first harmonic, the errors incurred by using (2) to relate the up/down wind brightness difference to an equivalent first harmonic coefficient should be minor. Results throughout the paper will thus be presented in terms of first harmonic coefficients derived from the up/down wind difference through (2) to facilitate comparisons with empirical models [17] for emission first harmonic coefficients.

The SSA expression for surface reflectivity is obtained by integrating standard small perturbation theory rough surface bistatic scattering coefficients over the upper hemisphere. Both "coherent" and "incoherent" reflectivity contributions exist at third-order for a surface with a nonvanishing bispectrum as described in [19]. Applying the scattering functions from [19], third-order brightness temperature corrections are

$$\Delta T_\gamma = -T_s \int dk_x \int dk_y \int dk_x' \int dk_y' \cdot 2\mathrm{Re}\{\Gamma(k_x, k_y, k_x', k_y') g_\gamma(k_x, k_y, k_x', k_y')\} \tag{3}$$

where $\Gamma(k_x, k_y, k_x', k_y')$ is the surface bispectrum and the g_γ "weighting" functions are given by

$$g_h = \mathrm{Re}\left\{ \frac{k_z''}{k_{zi}} \right\} \left(g_{hh}^{(1)*} g_{hh}^{(2)} + g_{vh}^{(1)*} g_{vh}^{(2)} \right) + g_{hh}^{(0)*} g_{hh}^{(3)} \tag{4}$$

$$g_v = \mathrm{Re}\left\{ \frac{k_z''}{k_{zi}} \right\} \left(g_{hv}^{(1)*} g_{hv}^{(2)} + g_{vv}^{(1)*} g_{vv}^{(2)} \right) + g_{vv}^{(0)*} g_{vv}^{(3)} \tag{5}$$

$$g_U = -\left[\mathrm{Re}\left\{\frac{k_z''}{k_{zi}}\right\}\left(g_{hh}^{(1)*}g_{hv}^{(2)} + g_{hv}^{(1)*}g_{hh}^{(2)} + g_{vv}^{(1)*}g_{vh}^{(2)} + g_{vh}^{(1)*}g_{vv}^{(2)}\right) + g_{hh}^{(0)*}g_{hv}^{(3)} + g_{vv}^{(0)*}g_{vh}^{(3)}\right] \quad (6)$$

$$g_V = -\left[\mathrm{Re}\left\{\frac{k_z''}{k_{zi}}\right\}\left(-g_{hh}^{(1)*}g_{hv}^{(2)} + g_{hv}^{(1)*}g_{hh}^{(2)} + g_{vv}^{(1)*}g_{vh}^{(2)} - g_{vh}^{(1)*}g_{vv}^{(2)}\right) - g_{hh}^{(0)*}g_{hv}^{(3)} + g_{vv}^{(0)*}g_{vh}^{(3)}\right]. \quad (7)$$

Note that $\mathrm{Re}\{\ \}$ in (3) is replaced by $\mathrm{Im}\{\ \}$ when calculating T_V, where $\mathrm{Re}\{\ \}$ and $\mathrm{Im}\{\ \}$ represent the real and imaginary part operators respectively. Also in the previous equations, $k_0 = 2\pi/\lambda$, λ is the electromagnetic wavelength, $k_{zi} = k\cos\theta_i$, $*$ represents the complex conjugate operation, and the g_γ functions are functions of f, θ_i, ϕ_i, and ϵ in addition to the four integration variables in (3). The $g_{\alpha\beta}^{(i)}$ SPM kernels in equations (4)–(7) are obtained from [19] and evaluated with arguments

$$g_{\alpha\beta}^{(1)}(k_x'', k_y'')$$
$$g_{\alpha\beta}^{(2)}(k_x'', k_y'', k_x' + k_{xi}, k_y' + k_{yi})$$
$$g_{\alpha\beta}^{(3)}(k_{xi}, k_{yi}, k_x + k_{xi}, k_y + k_{yi}, k_x' + k_{xi}, k_y' + k_{yi})$$

where $k_x'' = k_{xi} - k_x$, $k_y'' = k_{yi} - k_y$, $k_z'' = \sqrt{k_0^2 - k_x''^2 - k_y''^2}$, $k_{xi} = k_0\sin\theta_i\cos\phi_i$, and $k_{yi} = k_0\sin\theta_i\sin\phi_i$. Note that the second subscript $\beta = h, v$ refers to the incident polarization, while the first subscript α refers to the scattered polarization. Functions $g_{hh}^{(0)}$ and $g_{vv}^{(0)}$ are the horizontally and vertically polarized Fresnel reflection coefficients of a flat surface, respectively, as provided in [19]. Also, the integrals in (3) are all from $-\infty$ to ∞.

First azimuthal harmonics of surface brightness temperatures are obtained in the context of (2) by taking 0.5 ($\Delta T_\gamma(\phi_i = 0°) - \Delta T_\gamma(\phi_i = 180°)$) for linearly polarized brightness temperatures, 0.5 ($\Delta T_\gamma(\phi_i = 90°) - \Delta T_\gamma(\phi_i = 270°)$) for correlation brightness temperatures. First azimuthal harmonics then become

$$\Delta T_\gamma^{(1)} = 2T_s \int dk_x \int dk_y \int dk_x' \int dk_y' \cdot \mathrm{Im}\{\Gamma(k_x, k_y, k_x', k_y')\}\,\mathrm{Im}\{g_\gamma(k_x, k_y, k_x', k_y')\} \quad (8)$$

with the $\mathrm{Im}\{\ \}$ operator on g_γ replaced by $-\mathrm{Re}\{\ \}$ when $\Delta T_V^{(1)}$ is calculated; this replacement holds for all emission equations in the remainder of the paper. The previous g_γ functions are evaluated at $\phi_i = 0°$ for linearly polarized brightnesses and at $\phi_i = 90°$ for the correlation brightnesses. Equation (8) emphasizes that surface horizontal asymmetry is described only by the imaginary part of the bispectrum, as discussed in [24], [25]. A final simplification is obtained through symmetry considerations: Appendix A shows that the imaginary part of the bispectrum of a wind-generated sea surface has 24 symmetric regions. The emission weighting function g_γ can thus be symmetrized as described in Appendix A. All subsequent results assume that the symmetrized weighting functions are used.

Given a model for the sea surface bispectrum, (8) can be numerically integrated to obtain emission first azimuthal harmonics. At present however knowledge of the four dimensional sea surface bispectrum is very limited due to the difficulties associated with measurement of this quantity. Thus a direct evaluation of (8) is not meaningful at this time. Approximations that simplify (8) to capture the contributions of long wave asymmetry and long-short wave modulations are considered in the next sections.

III. Approximation for Large-Scale Wave Contributions

For surfaces composed only of waves whose length is much greater than the electromagnetic wavelength, nonzero values in the surface bispectrum will be located in regions where all integration variables in (8) are $\ll k_0$. A Taylor series expansion of the emission weighting function is then possible as

$$g_\gamma(k_x, k_y, k_x', k_y') \approx g_\gamma(0,0,0,0) + k_x\, g_{\gamma,k_x}(0,0,0,0) + k_y\, g_{\gamma,k_y}(0,0,0,0) + \cdots \quad (9)$$

where the additional subscripts refer to the corresponding derivatives of the g_γ function evaluated at the origin. Zeroth, first, and second-order term contributions from this Taylor series in (8) are found to vanish identically due to properties of the symmetrized g_γ functions. At third-order, twenty terms are obtained but symmetry properties cause the contributions of 14 of these to vanish. Relationships between contributions from the remaining six terms can also be found, so that only two distinct terms remain in the final result

$$\Delta T_\gamma^{(1)} \approx 2T_s\Big(\mathrm{Im}\{g_{\gamma,k_x,k_x,k_x'}\}\int dk_x \int dk_y \int dk_x' \int dk_y' \cdot k_x' k_x^2 \cdot \mathrm{Im}\{\Gamma(k_x, k_y, k_x', k_y')\} + \mathrm{Im}\Big\{g_{\gamma,k_x',k_y,k_y} + 2g_{\gamma,k_x,k_y,k_y'}\Big\} \cdot \int dk_x \int dk_y \int dk_x' \int dk_y' \cdot k_x' k_y^2\,\mathrm{Im}\{\Gamma(k_x, k_y, k_x', k_y')\}\Big). \quad (10)$$

The results can be further simplified through a process similar to that described in [26], which shows that

$$\int dk_x \int dk_y \int dk_x' \int dk_y'\, k_x' k_x^2\,\mathrm{Im}\{\Gamma(k_x, k_y, k_x', k_y')\} = -\tfrac{1}{2}\langle z_x^3\rangle \quad (11)$$

$$\int dk_x \int dk_y \int dk_x' \int dk_y'\, k_x' k_y^2\,\mathrm{Im}\{\Gamma(k_x, k_y, k_x', k_y')\} = -\tfrac{1}{2}\langle z_x z_y^2\rangle \quad (12)$$

where $\langle z_x^3\rangle$ refers to the third moment of surface upwind slopes, and $\langle z_x z_y^2\rangle$ refers to the correlation of surface upwind slope with

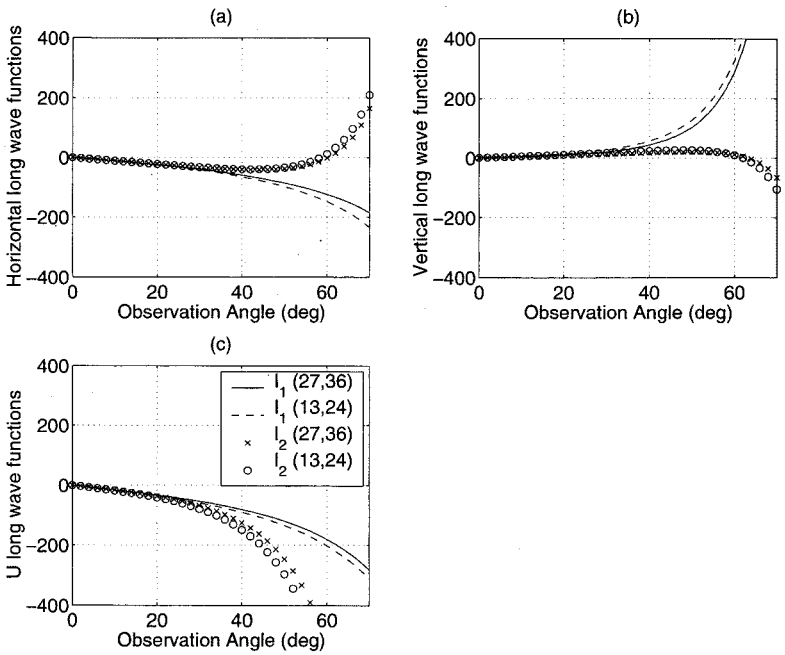

Fig. 1. Long wave functions $T_s\, l_1$ and $T_s\, l_2$ for surface permittivities of $27 + i36$ and $13 + i24$. (a) Horizontal, (b) vertical, and (c) U.

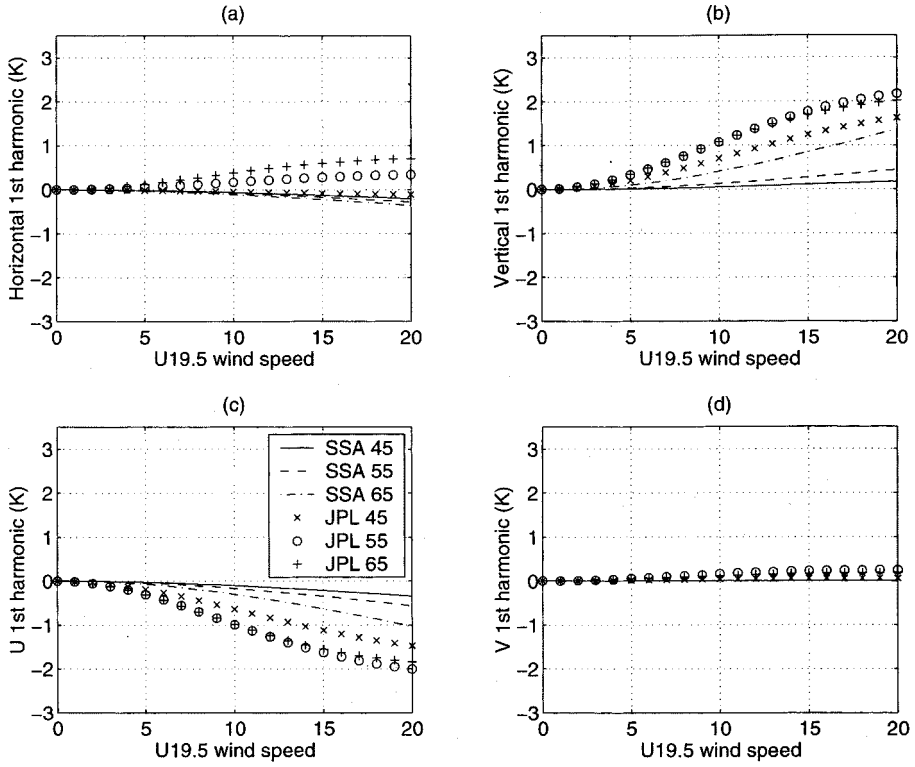

Fig. 2. Comparison of long wave first harmonics with JPL WindRAD empirical model at 19.35 GHz. (a) Horizontal, (b) vertical, (c) U, and (d) V.

crosswind slope squared. The final expression for long wave contributions is then

$$\Delta T_\gamma^{(1)} \approx -T_s\Big(\mathrm{Im}\left\{g_{\gamma,k_x,k_x,k_x'}\right\}\langle z_x^3\rangle + \mathrm{Im}\Big\{g_{\gamma,k_x',k_y,k_y} + 2g_{\gamma,k_x,k_y,k_y'}\Big\}\langle z_x z_y^2\rangle\Big) \quad (13)$$

$$= T_s\left(l_1(\theta_i,\epsilon)\langle z_x^3\rangle + l_2(\theta_i,\epsilon)\langle z_x z_y^2\rangle\right) \quad (14)$$

which confirms the small slope nature of the approximation.

Note that surface and emission effects are decoupled into a product form in the large scale surface limit. The only properties of the surface that are required for first azimuthal harmonic calculations are the moments $\langle z_x^3\rangle$ and $\langle z_x z_y^2\rangle$. First harmonic variations with polar observation angle and surface permittivity are all contained in the third derivative functions redefined as l_1 and l_2 earlier: angular and permittivity variations are simply scaled by the slope moments for differing surface shapes. The

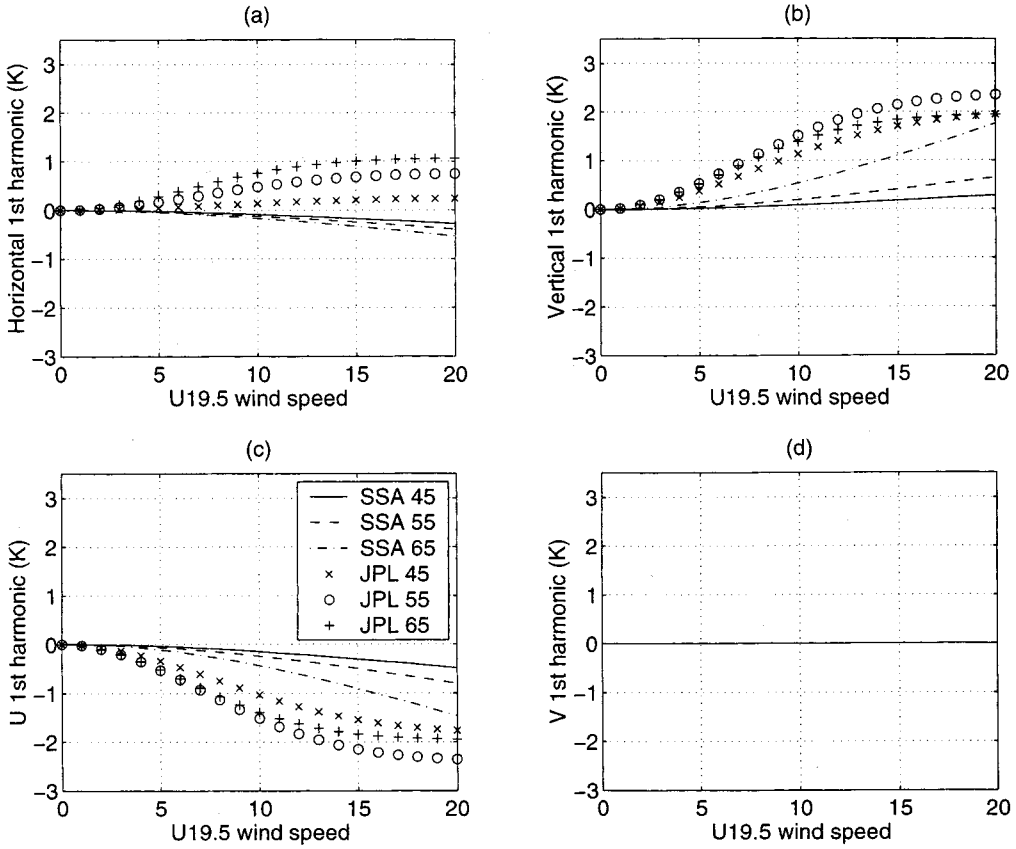

Fig. 3. Comparison of long wave first harmonics with JPL WindRAD empirical model at 37 GHz. (a) Horizontal, (b) vertical, (c) U, and (d) V (empirical model not available for V).

l_1 and l_2 functions in (14) are also found to be independent of the radiometer frequency, illustrating that an optical type limit is obtained, and both functions vanish for the fourth Stokes parameter as should be expected in an optical limit. A more detailed discussion of the relationship between these results and optical theories is provided in [27].

Fig. 1 plots $T_s\, l_1$ and $T_s\, l_2$ versus polar observation angle for sea water permittivities $27 + i36$ at 19 GHz and $13 + i24$ at 37 GHz [28]. In general, l_1 is observed to have a larger amplitude than l_2 for linearly polarized brightnesses, while l_2 appears more important for U brightnesses. The l_1 and l_2 functions have the same signs for small to moderate observation angles but have opposite signs for linearly polarized brightnesses at larger observation angles. All curves show the expected trends of increasing amplitude as polar angle increases and vanish at nadir observation as required by symmetry [23].

Estimates of the moments $\langle z_x^3 \rangle$ and $\langle z_x z_y^2 \rangle$ for the sea surface are available from the optical measurements of [29] (also described in [30])

$$\langle z_x^3 \rangle \approx - \left(\langle z_x^2 \rangle \right)^{1.5} (0.04 - 0.033W) \tag{15}$$

$$\langle z_x z_y^2 \rangle \approx - \left(\langle z_x^2 \rangle \right)^{0.5} \langle z_y^2 \rangle (0.01 - 0.0086W) \tag{16}$$

where W represents the surface wind speed in m/s at 19.5 m altitude. Note, however, that the large scale approximation requires that only surface length scales much larger than the electromagnetic wavelength be included in the calculation of $\langle z_x^3 \rangle$ and $\langle z_x z_y^2 \rangle$, whereas the data of [29] may include contributions from shorter waves. Thus, moments obtained from [29] should serve as upper limits on the desired moments in the large scale approximation. Reference [29] also provides estimates of the mean square surface slopes $\langle z_x^2 \rangle$ and $\langle z_y^2 \rangle$, but these can instead be obtained from the long wave portion of a model of the sea-surface directional spectrum such as that of [31]. In the results to be shown, long-wave slope variances were obtained from waves in the ocean surface larger than 20 electromagnetic wavelengths.

Figs. 2 and 3 compare first azimuthal harmonics obtained from the large scale approximation with the WindRAD empirical model from Jet Propulsion Laboratory (JPL) measurements [17] versus wind speed. The WindRAD model applies for brightnesses at 19.35 GHz (Fig. 2) and 37 GHz (Fig. 3) and for polar observation angles 45°, 55°, and 65°. In general, Figs. 2 and 3 show that long wave asymmetry effects alone underestimate empirical results and predict an opposite sign for horizontally polarized first azimuthal harmonics in most cases. Long-wave contributions appear to be most important at larger windspeeds, where long wave asymmetry becomes more pronounced. Similar results are obtained with other models of the surface spectrum [32], [33]. Slope moments obtained from the spectrum of [31] are in fact the largest of the three spectra considered, so the data in Figs. 2 and 3 again are expected to overestimate large scale region contributions. These results show that long wave asymmetry effects can contribute to sea surface first

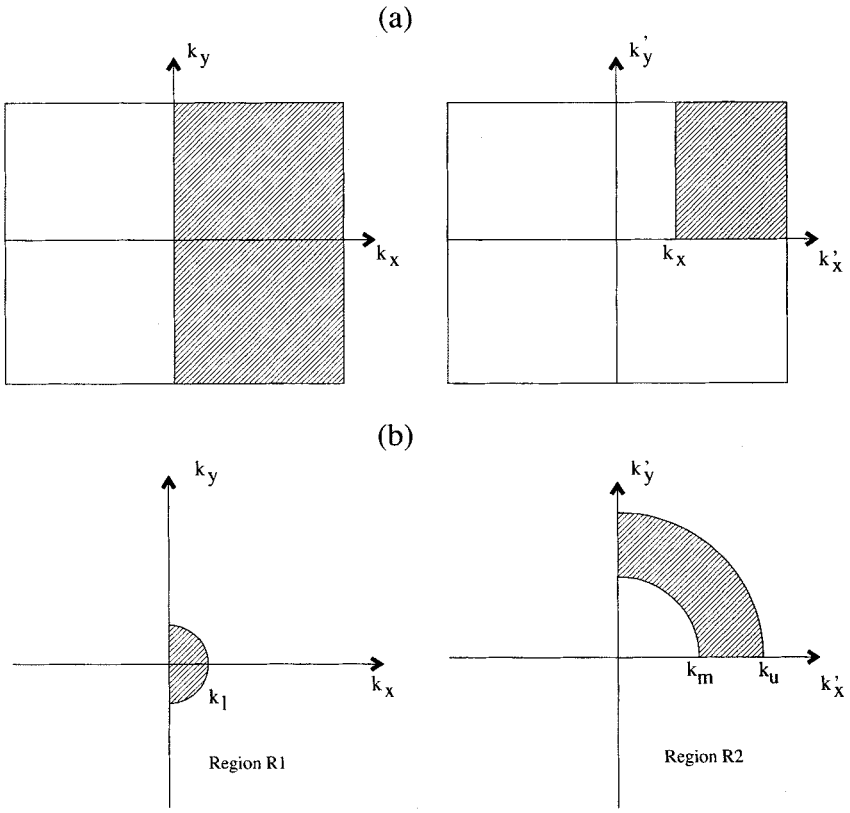

Fig. 4. Integration regions for long-short wave approximation. (a) Original minimum region and (b) approximation region.

azimuthal harmonics at larger wind speeds, but other mechanisms are required as well in order to reproduce measured data.

IV. Approximation for Modulated Short Waves

A second approximation can be derived if it is assumed that only the first two of four integration variables in (8) are small compared to k_0, while the second pair is much larger than the first pair. Note the second pair of integration variables is not assumed to have any particular relationship with the electromagnetic wavelength. The approximation requires that symmetry properties of the bispectrum are used to reduce the integration region to the minimum region discussed in Appendix A, i.e., $k'_x > k_x > 0$, $k'_y > 0$. In this case, the assumption $k'_\rho \gg k_\rho$ where $k_\rho = \sqrt{k_x^2 + k_y^2}$ and $k'_\rho = \sqrt{k_x'^2 + k_y'^2}$ is reasonable for a portion of the minimum region that corresponds to short waves modulated by longer waves. Fig. 4 illustrates the original minimum region and the portion captured [defined as regions R_1 and R_2 in the (k_x, k_y) and (k'_x, k'_y) planes, respectively] by the modulated short wave approximation. Note the original minimum region boundary $k'_x > k_x$ is replaced by $k'_\rho > k_m \gg k_l$, $k_\rho < k_l \ll k_0$ for simplicity in the approximation.A Taylor series expansion in k_x and k_y is now applied in (8) to obtain

$$\begin{aligned}\Delta T_\gamma^{(1)} \approx 48 T_s \int_{R_1} dk_x \int dk_y \int_{R_2} dk'_x \int dk'_y \\ \cdot \operatorname{Im}\{\Gamma(k_x, k_y, k'_x, k'_y)\} \\ \cdot \operatorname{Im}\{g_\gamma(0, 0, k'_x, k'_y) + k_x g_{\gamma, k_x}(0, 0, k'_x, k'_y) \\ + k_y g_{\gamma, k_y}(0, 0, k'_x, k'_y) + \cdots\}. \end{aligned} \quad (17)$$

Symmetry properties of the g_γ functions cause the zeroth-order term to vanish, leaving

$$\begin{aligned}\Delta T_\gamma^{(1)} \approx 48 T_s \Bigg[\int_{R_2} dk'_x \int dk'_y \operatorname{Im}\{g_{\gamma, k_x}(0, 0, k'_x, k'_y)\} \\ \cdot \int_{R_1} dk_x \int dk_y \, k_x \operatorname{Im}\{\Gamma(k_x, k_y, k'_x, k'_y)\} \\ + \int_{R_2} dk'_x \int dk'_y \operatorname{Im}\{g_{\gamma, k_y}(0, 0, k'_x, k'_y)\} \\ \cdot \int_{R_1} dk_x \int dk_y \, k_y \operatorname{Im}\{\Gamma(k_x, k_y, k'_x, k'_y)\} \Bigg] \\ = 48 T_s \Bigg[\int_{R_2} dk'_x \int dk'_y \operatorname{Im}\{g_{\gamma, k_x}(0, 0, k'_x, k'_y)\} \\ \cdot R_x(k'_x, k'_y) + \operatorname{Im}\{g_{\gamma, k_x}(0, 0, k'_x, k'_y)\} \\ \cdot R_y(k'_x, k'_y) \Bigg] \end{aligned} \quad (18)$$

where "reduced bispectra" are defined as

$$R_x(k'_x, k'_y) = \int_{R_1} dk_x \int dk_y \, k_x \operatorname{Im}\{\Gamma(k_x, k_y, k'_x, k'_y)\} \quad (19)$$

$$R_y(k'_x, k'_y) = \int_{R_1} dk_x \int dk_y \, k_y \operatorname{Im}\{\Gamma(k_x, k_y, k'_x, k'_y)\} \quad (20)$$

for k'_x and k'_y in region R_2. Thus, the approximation decouples the four fold integral into a double integral over the bispectrum to obtain new "reduced bispectra" surface descriptors,

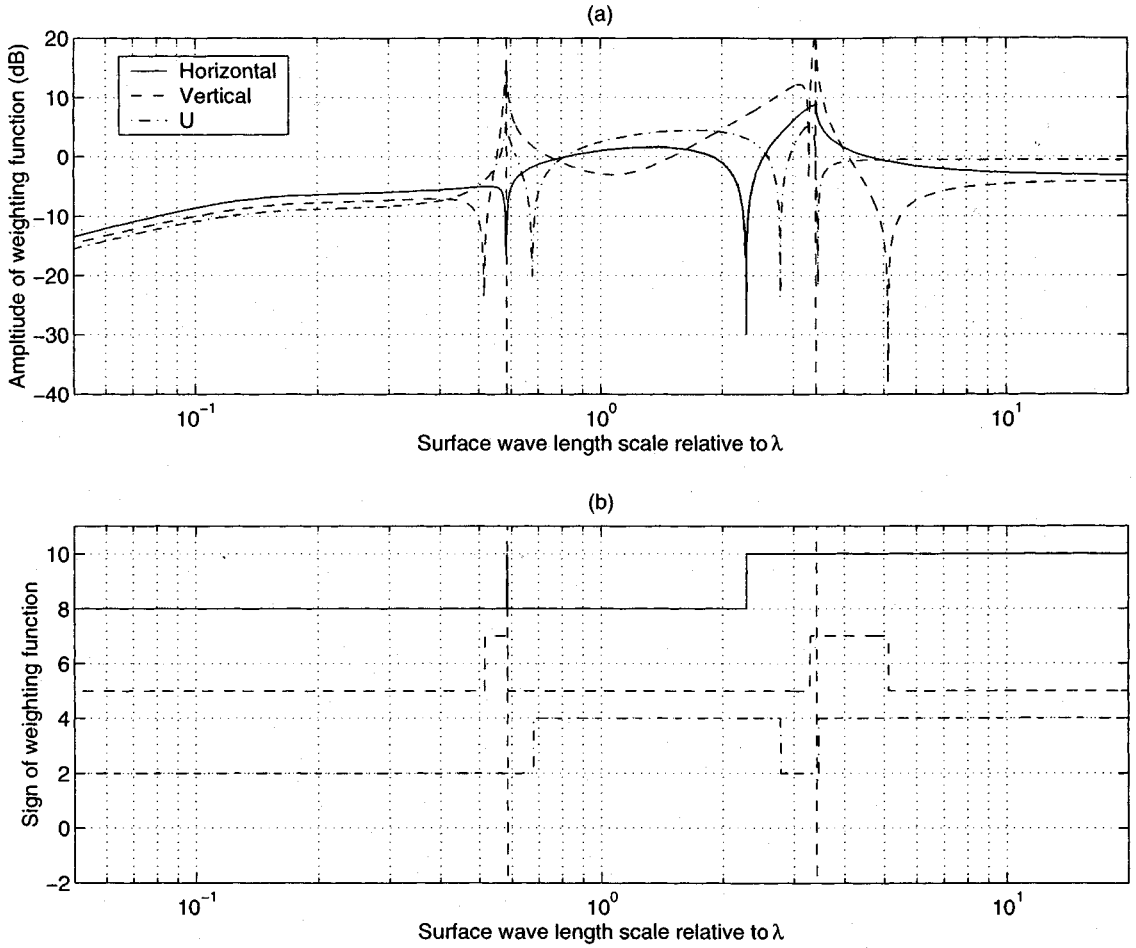

Fig. 5. Weighting functions $g^0_{\gamma,k_x}/k'^2_\rho$ versus ocean wave length scale relative to the electromagnetic wavelength for sea water permittivity $27 + i36$ and observation angle 45°. (a) Magnitudes of weighting functions in dB and (b) signs of weighting functions. Note sign curves for horizontal, vertical, and U polarizations are shifted by $+9$, $+6$, and $+3$, respectively.

combined with a double integral over the reduced bispectra multiplied with a pair of new emission weighting functions. Evaluation of (18) is thus simpler than (8) if reasonable models for surface reduced bispectra can be developed. Note the reduced bispectra defined here are identical to the two argument bispectra of [24], [25] if the k_x and k_y multipliers in equations (19) and (20) are neglected, respectively.

It can be shown that $R_x(k'_x, k'_y) = R_x(k'_x, -k'_y)$, $R_y(k'_x, k'_y) = -R_y(k'_x, -k'_y)$ due to symmetries of the bispectrum and region R_1. If R_x and R_y are further defined to be even under a sign change in k'_x (outside the region R_2) then these functions can be expanded in a series of azimuthal harmonics as

$$R_x(k'_\rho, \phi') = \sum_{n=0}^{\infty} R_{xn}(k'_\rho)\cos 2n\phi' \tag{21}$$

$$R_y(k'_\rho, \phi') = \sum_{n=0}^{\infty} R_{yn}(k'_\rho)\sin(2n+1)\phi'. \tag{22}$$

The weighting functions g_{γ,k_x} and g_{γ,k_y} can be defined to possess the same symmetries, so the first quadrant integral in region R_2 can be modified to all four quadrants if the result is divided by four. Substituting the azimuthal bispectra expansions into (18) and further defining

$$g^n_{\gamma,k_x}(k'_\rho) = \int_0^{2\pi} d\phi' \,\mathrm{Im}\left\{g_{\gamma,k_x}(0, 0, k'_\rho, \phi')\right\}\cos 2n\phi' \tag{23}$$

$$g^n_{\gamma,k_y}(k'_\rho) = \int_0^{2\pi} d\phi' \,\mathrm{Im}\left\{g_{\gamma,k_y}(0, 0, k'_\rho, \phi')\right\}\sin(2n+1)\phi' \tag{24}$$

results in

$$\Delta T^{(1)}_\gamma = 12T_s\left\{\sum_{n=0}^{\infty}\int_{k_m}^{k_u} dk'_\rho\, k'_\rho\left[R_{xn}(k'_\rho)g^n_{\gamma,k_x}(k'_\rho) + R_{yn}(k'_\rho)g^n_{\gamma,k_y}(k'_\rho)\right]\right\} \tag{25}$$

with k_u included as an upper boundary for a numerical integration. The azimuthal integrals in (23) and (24) can involve rapidly varying functions when k'_ρ lies in the "critical phenomenon" region described below, so care must be exercised in evaluating these integrals.

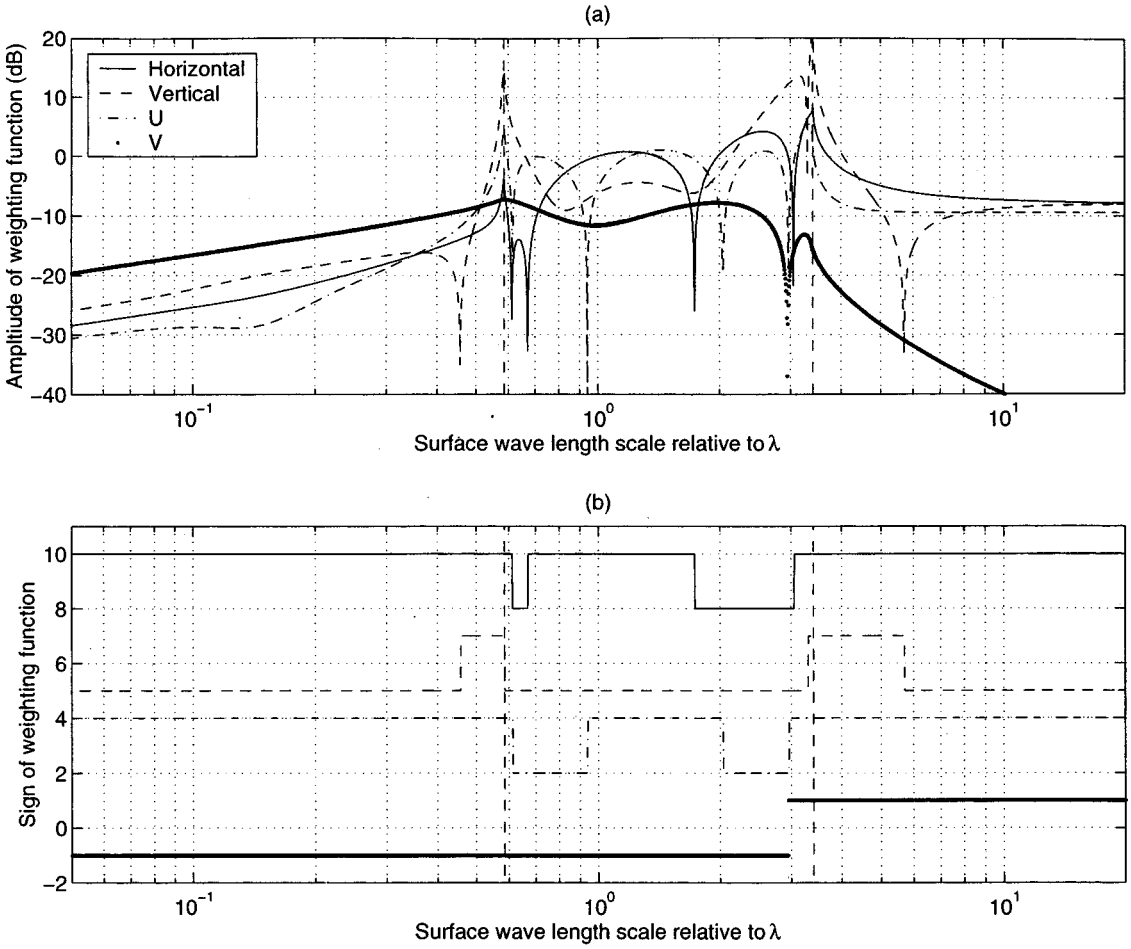

Fig. 6. Weighting functions $g^1_{\gamma,\,k_x}/k'^2_\rho$ versus ocean wave length scale relative to the electromagnetic wavelength for sea water permittivity $27 + i36$ and observation angle 45°. (a) Magnitudes of weighting functions in dB and (b) signs of weighting functions. Note sign curves for horizontal, vertical, and U polarizations are shifted by $+9$, $+6$, and $+3$, respectively.

To enable plots of the weighting functions for a large range of length scales, the substitution $k'_\rho = k_0/10^q$ is made and the integral rewritten over $q = \log_{10}(k_0/k'_\rho)$. Also the reduced bispectra are replaced with unitless reduced "curvature" bispectra, defined as $C_{jn}(k'_\rho) = k'^4_\rho R_{jn}(k'_\rho)$ for $j = x$ or y. The final form of (25) is then

$$\Delta T^{(1)}_\gamma = 12\,T_s(\ln 10)\left\{\sum_{n=0}^{\infty}\int_{q_a}^{q_m} dq\left[C_{xn}(k'_\rho)\,\frac{g^n_{\gamma,k_x}(k'_\rho)}{k'^2_\rho} + C_{yn}(k'_\rho)\,\frac{g^n_{\gamma,k_y}(k'_\rho)}{k'^2_\rho}\right]\right\}. \tag{26}$$

In the previous equation, the unitless quantities $g^n_{\gamma,\,k_x}/k'^2_\rho$ and $g^n_{\gamma,\,k_y}/k'^2_\rho$ provide the relative contributions of differing length scales in the reduced curvature bispectra when integrated over a logarithmic axis.

Figs. 5–7 illustrate the $g^0_{\gamma,\,k_x}/k'^2_\rho$, $g^1_{\gamma,\,k_x}/k'^2_\rho$, and $g^0_{\gamma,\,k_y}/k'^2_\rho$ functions respectively versus surface wave length scale relative to the electromagnetic wavelength for a 19.35 GHz sea water permittivity at observation angle 45°. Functions for all four polarizations are included in these figures (excepting the fourth Stokes parameter in Fig. 5 whose amplitude is negligibly small), with magnitudes of the functions in dB and their signs (defined as $+1$ for positive values, -1 for negative values) illustrated in separate plots. Note the sign curves for differing polarizations are shifted to allow them to be more easily distinguished. These functions are independent of the observation frequency when plotted versus length scale relative to the electromagnetic wavelength, except for variations which would occur in surface permittivity. The plots are truncated at a maximum length scale of twenty electromagnetic wavelengths, since the modulating long waves inherent in this approximation must be much longer than the "short" waves illustrated, and include results up to one twentieth of the electromagnetic wavelength. Note the "critical phenomenon" resonance type effects [18], [34] that are observed for length scales on the order of the electromagnetic wavelength. The vertical lines in the figures mark the boundaries of this region. Magnitudes of the weighting functions in this region are observed to be quite large in some instances, suggesting that modulated short waves in the critical phenomenon region can potentially be the dominant contributors of long–short wave modulation induced first azimuthal harmonics. However, the magnitude of the contribution will depend also on the amplitude of the reduced curvature bispectra in this region. Note also that in some regions, the weighting functions show similar signs

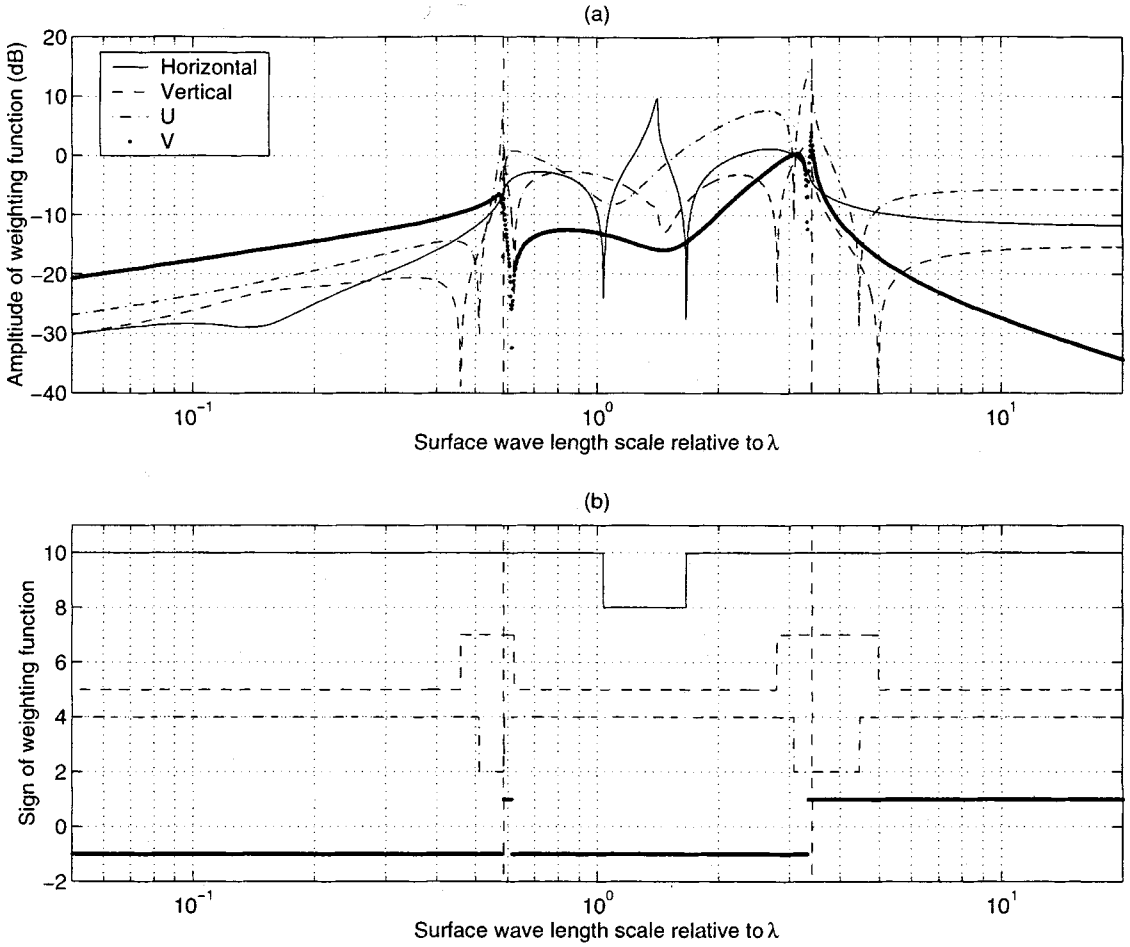

Fig. 7. Weighting functions $g^0_{\gamma,k_y}/k'^2_\rho$ versus ocean wave length scale relative to the electromagnetic wavelength for sea water permittivity $27 + i36$ and observation angle 45°. (a) Magnitudes of weighting functions in dB and (b) signs of weighting functions. Note sign curves for horizontal, vertical, and U polarizations are shifted by $+9$, $+6$, and $+3$, respectively.

for horizontal and vertically polarized functions so that correct polarization dependencies can be captured under this approximation for a subset of possible reduced bispectra functions.

To further explore the modulated short-wave approximation, calculations are performed for the reduced bispectra models described in Appendix B: those of [8] and [35]. The model of [8] was empirically derived to fit measured emission first harmonic data under a composite surface model, and cannot necessarily be considered a complete hydrodynamic model. The model of [35] is derived based on the "modulation transfer function" of weak hydrodynamic theory [36] and should thus model hydrodynamic effects more realistically. When comparing with JPL WindRAD measurements at 19.35 and 37 GHz, however, short waves in the critical phenomenon region occur near the 1.55 cm and 8.1 mm electromagnetic wavelengths for which the current weak hydrodynamic theory is known to underpredict hydrodynamic modulations [36], particularly at low to moderate wind speeds. Thus at present, an effective hydrodynamic model for reduced bispectra at the length scales of interest is not available. Figs. 8 and 9 illustrate comparisons with the WindRAD empirical model at 19.35 GHz for the [8] and [35] reduced bispectra models, respectively, using the sea surface spectral model of [33]. The integral in (26) included contributions for $n = 0$, 1, and 2, and was performed over the range of length scales illustrated in Figs. 5–7 with "long" waves defined as those longer than one meter. The empirically derived model of [8] is observed to continue to match data well under the third-order SSA, although amplitudes at the smaller observation angles and for the fourth Stokes parameter are underpredicted. The weak hydrodynamic theory model significantly underpredicts all measured data as expected.

V. Conclusions

A complete third-order SSA theory for prediction of the up/down wind asymmetry of sea surface brightness temperatures has been derived and presented in this paper. The resulting expressions are difficult to evaluate due to limited present knowledge of the sea surface bispectrum, but approximations to obtain the contributions of surface length scales much greater than the electromagnetic wavelength or contributions of short waves modulated by longer waves allow some insights to be obtained. The large-scale surface approximation shows that only third moments of the surface slope are required to describe surface properties, but the resulting first harmonics obtained underestimate those of measured data and do not capture the correct polarization dependencies. The modulated wave approximation produces a double integration over surface

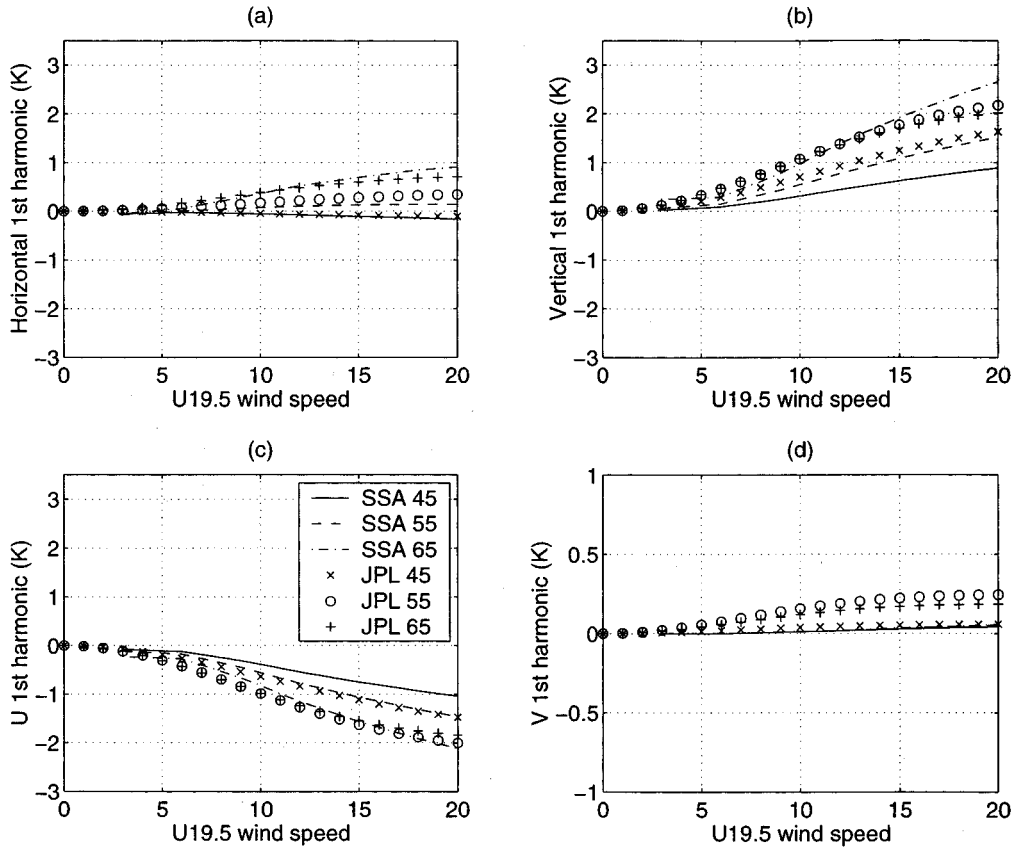

Fig. 8. Comparison of modulated short wave first harmonics with JPL WindRAD empirical model at 19.35 GHz, using the [8] reduced bispectra: (a) horizontal, (b) vertical, (c) U, (d) V.

"reduced bispectra," and studies of the weighting functions in this limit illustrate the importance of critical phenomena effects for surface length scales on the order of the electromagnetic wavelength. Comparisons with measured data in this limit, however, are limited by the absence of an effective model for centimeter scale wave modulation by longer waves and wind effects. The conclusions of this paper parallel those of [18] in suggesting that both long wave and long–short wave modulation effects can contribute to observed up/down wind emission differences and motivate further hydrodynamic studies of short-wave modulation. Research applying numerical models for nonlinear hydrodynamic evolution of sea surfaces [37] is also of interest for obtaining improved models of the sea surface bispectrum. Surface foam effects should also be further studied to determine their relative influence.

Appendix A
Properties of the Bispectrum

For a random process $z(x, y)$, the bispectrum $\Gamma(k_x, k_y, k_x', k_y')$ is the next-order statistic following the second-order surface power spectrum and is defined as the Fourier transform (FT) of the surface bicorrelation function

$$\rho_3(x, y, x', y') = \langle z(\alpha, \beta) z(\alpha + x, \beta + y) z(\alpha + x', \beta + y') \rangle . \quad (27)$$

For a random process with FT $\tilde{z}(k_x, k_y)$ (defined in the Fourier–Stieltjes integral sense), the bispectrum can also be expressed as

$$\Gamma(k_x, k_y, k_x', k_y') = \left\langle \tilde{z}(k_x, k_y) \tilde{z}(k_x', k_y') \tilde{z}(-k_x - k_x', -k_y - k_y') \right\rangle . \quad (28)$$

The previous definition, along with the fact that $z(x, y)$ is real-valued, makes the following symmetry properties apparent:

$$\Gamma(k_x, k_y, k_x', k_y') = \Gamma(k_x', k_y', k_x, k_y) \quad (29)$$

$$= \Gamma^*(-k_x, -k_y, -k_x', -k_y') \quad (30)$$

$$= \Gamma(-k_x - k_x', -k_y - k_y', k_x', k_y') \quad (31)$$

$$= \Gamma(k_x, k_y, -k_x - k_x', -k_y - k_y'). \quad (32)$$

Symmetry properties (29) and (30) combine to produce four symmetry regions, while properties (31) and (32) produce only three, resulting in a total of 12 symmetry regions for a general bispectrum. For a wind-generated sea surface (without swell), a symmetry of the FT in the cross-wind direction can also be assumed, leading to

$$\Gamma(k_x, k_y, k_x', k_y') = \Gamma(k_x, -k_y, k_x', -k_y') \quad (33)$$

for a total of 24 symmetric regions. An analysis similar to that for discrete random processes in [38] can be used to determine

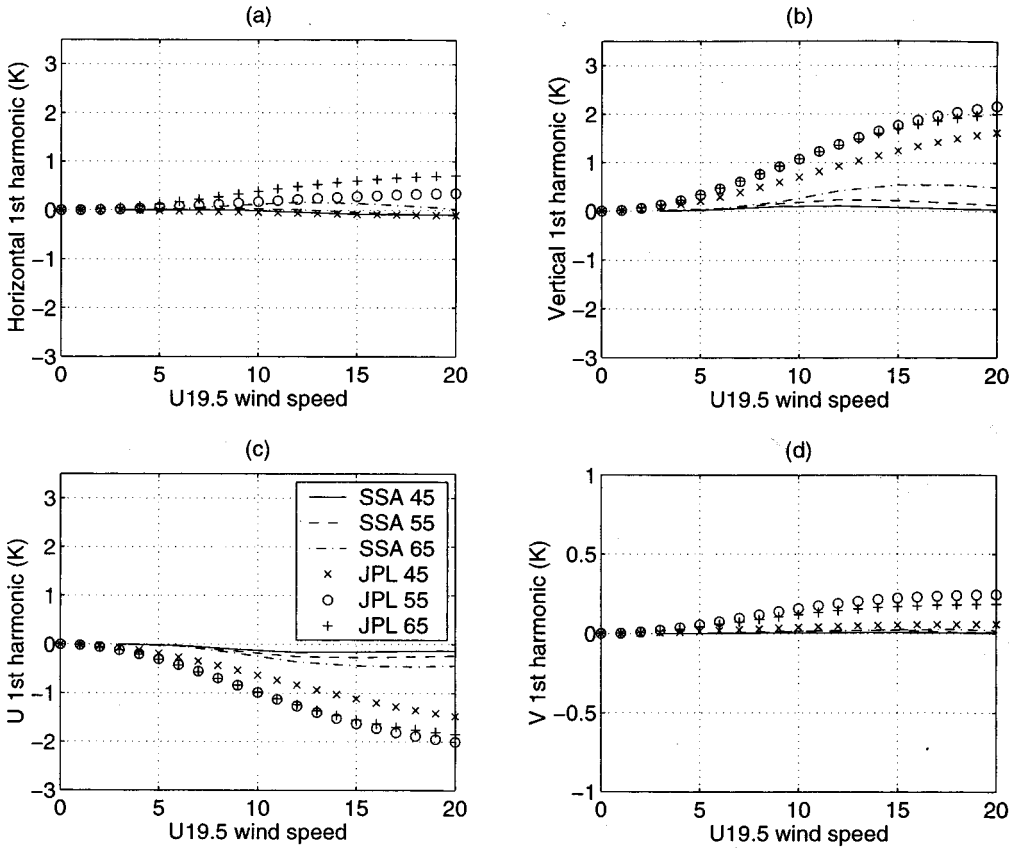

Fig. 9. Comparison of modulated short wave first harmonics with JPL WindRAD empirical model at 19.35 GHz, using the [35] reduced bispectra: (a) horizontal, (b) vertical, (c) U, and (d) V.

the minimum region of 4-D space needed for complete determination of the bispectrum. The resulting minimum region can be specified as $k'_x > k_x > 0$, $k'_y > 0$ and is illustrated in Fig. 4.

Note that functions that multiply a bispectrum in an integration over all arguments can be replaced by a 24-term symmetrized version of the original function, since terms without the correct symmetries will vanish in the integration. The symmetrized integral over all space can then be replaced with 24 times the integral over the minimum region.

Appendix B
Reduced Bispectra for Modulated Surfaces

Models for the bispectrum of a modulated sea surface can be derived if a weak interaction between independent Gaussian random processes $l(x, y)$ (the long-wave portion of the surface), and $s_0(x, y)$ (the unmodulated short wave portion of the surface) is assumed. FTs of these processes are defined as $\tilde{l}(k_x, k_y)$ and $\tilde{s}_0(k_x, k_y)$, respectively.

First consider the modulation model applied in [8], in which the spectrum of short waves is multiplied by a linear function $m = 1 + b l_x$ of long wave along wind slope, where $b = 0.4/\sqrt{\langle l_x^2 \rangle}$ is constant in space, and l_x is the upwind slope of the long-wave process. The modulation m is also limited in [8] at amplitudes 0.5 and 1.5. If the amplitude limits of this function are neglected, and the modulated short-wave process $s(x, y)$ in the space domain is written as

$$s(x, y) = \sqrt{1 + b\, l_x(x, y)}\, s_0(x, y) \tag{34}$$

$$\approx \left(1 + \frac{b}{2} l_x(x, y)\right) s_0(x, y) \tag{35}$$

$$= s_0(x, y) + s_1(x, y) \tag{36}$$

the FT of the modulated total process can be written as

$$\tilde{z}(k_x, k_y) = \tilde{l}(k_x, k_y) + \tilde{s}_0(k_x, k_y) + \frac{b}{2} \int dk'_x \int dk'_y\, i k'_x \tilde{l}(k'_x, k'_y)\, \tilde{s}_0(k_x - k'_x, k_y - k'_y). \tag{37}$$

The resulting bispectrum from (28) is then

$$\begin{aligned} \Gamma\left(\overline{k}, \overline{k}'\right) = i \frac{b}{2} \big[& -k_x W_l(\overline{k}) W_s\left(\overline{k}'\right) - k'_x W_l\left(\overline{k}'\right) W_s(\overline{k}) \\ & - k_x W_l(\overline{k}) W_s\left(\overline{k} + \overline{k}'\right) \\ & - k'_x W_l\left(\overline{k}'\right) W_s\left(\overline{k} + \overline{k}'\right) \\ & + (k_x + k'_x) W_l\left(\overline{k} + \overline{k}'\right) W_s(\overline{k}) \\ & + (k_x + k'_x) W_l\left(\overline{k} + \overline{k}'\right) W_s(\overline{k}) \big] \end{aligned} \tag{38}$$

which satisfies all the symmetry properties described in Appendix A. W_l and W_s described earlier are the long and short-wave directional spectra, respectively. Note if it is assumed that $\overline{k}$ corresponds to long waves while $\overline{k}'$ corresponds to short waves, as in the long-short wave approximation, only the first and third terms are nonzero

$$\begin{aligned} \Gamma\left(\overline{k}, \overline{k}'\right) \approx i \frac{b}{2} \big[& -k_x W_l(\overline{k}) W_s\left(\overline{k}'\right) \\ & - k_x W_l(\overline{k}) W_s\left(\overline{k} + \overline{k}'\right) \big] \end{aligned} \tag{39}$$

$$\approx -i\,b\,k_x\,W_l(\overline{k})W_s\left(\overline{k}'\right). \tag{40}$$

The additional approximation to obtain (40) previously is reasonable since $|\overline{k}|$ should be smaller than $|\overline{k}'|$. The reduced bispectra from equations (19), (20) for the long-short wave approximation then become

$$R_x\left(\overline{k}'\right) \approx -\langle l_x^2\rangle\,\frac{b}{2}\,W_s\left(\overline{k}'\right) = -0.2\sqrt{\langle l_x^2\rangle}\,W_s\left(\overline{k}'\right) \tag{41}$$

$$R_y\left(\overline{k}'\right) \approx 0 \tag{42}$$

where $\langle l_x^2\rangle$ is the long wavesurface along wind slope variance. Equation (18) thus becomes an integral over the short-wave directional spectrum in this approximation.

A more realistic hydrodynamic model can be obtained from the "modulation transfer function" of weak interaction theory, as described in [35]. Similar arguments that replace modulations of the short wave spectrum with modulations of space domain short waves can be used to show that the bispectrum is approximately

$$\Gamma\left(\overline{k},\,\overline{k}'\right) \approx \tfrac{1}{2}\left[R_{\overline{k},\,\overline{k}'}W_l(\overline{k})W_s\left(\overline{k}'\right) + R_{\overline{k},\,\overline{k}+\overline{k}'}W_l(\overline{k})W_s\left(\overline{k}+\overline{k}'\right)\right] \tag{43}$$

$$\approx R_{\overline{k},\,\overline{k}'}W_l(\overline{k})W_s\left(\overline{k}'\right) \tag{44}$$

where $R_{\overline{k},\,\overline{k}'}$ is the hydrodynamic modulation transfer function (HMTF) as defined in [35] (related to $1/|\overline{k}|$ times the HMTF of [36]). A similar relationship between the HMTF and surface bispectrum was derived in [18]. Since $R_{\overline{k},\,\overline{k}'}$ is not a simple function and is not separable in $\overline{k}$ and $\overline{k}'$, a numerical integration is required in (19) and (20) to obtain the reduced bispectra for each value of $\overline{k}'$. In the results shown, the wind growth parameter of [39] was applied with a quadratic restoring force, and all waves were assumed to travel in the downwind direction. Note (40) is equivalent to (44) if the imaginary part of the modulation transfer function is modeled as $-(0.4/\sqrt{\langle l_x^2\rangle})k_x$. This amplitude is not unreasonable when compared with the measured data of [36].

ACKNOWLEDGMENT

A prepublished copy of [35] provided by its authors is appreciated.

REFERENCES

[1] M. S. Dzura, V. S. Etkin, A. S. Khrupin, M. N. Pospelov, and M. D. Raev, "Radiometers polarimeters: Principles of design and applications for sea surface microwave emission polarimetry," in *Proc. IGARSS'92 Conf.*, Houston, TX, 1992, pp. 1432–1434.

[2] F. J. Wentz, "Measurement of oceanic wind vector using satellite microwave radiometers," *IEEE Trans. Geosci. Remote Sensing*, vol. 30, pp. 960–972, 1992.

[3] S. H. Yueh, W. J. Wilson, F. K. Li, S. V. Nghiem, and W. B. Ricketts, "Polarimetric measurements of sea surface brightness temperatures using an aircraft K-band radiometer," *IEEE Trans. Geosci. Remote Sensing*, vol. 33, pp. 85–92, 1995.

[4] J. R. Piepmeier and A. J. Gasiewski, "High-resolution passive polarimetric microwave mapping of ocean surface wind vector fields," *IEEE Trans. Geosci. Remote Sensing*, vol. 39, pp. 606–622, 2001.

[5] S. D. Gasster and G. M. Flaming, "Overview of the conical microwave imager/sounder development for the NPOESS program," in *Proc. IGARSS'98*, vol. 1, Seattle, WA, 1998, pp. 268–271.

[6] K. M. St. Germain and P. W. Gaiser, "Spaceborne polarimetric microwave radiometry and the Coriolis WindSat system," *Proc. IEEE Aerospace Conf.*, vol. 5, pp. 159–164, 2000.

[7] S. H. Yueh, R. Kwok, F. K. Li, S. V. Nghiem, and W. J. Wilson, "Polarimetric passive remote sensing of ocean wind vectors," *Radio Sci.*, vol. 29, pp. 799–814, 1994.

[8] S. H. Yueh, "Modeling of wind direction signals in polarimetric sea surface brightness temperatures," *IEEE Trans. Geosci. Remote Sensing*, vol. 35, pp. 1400–1418, Nov. 1997.

[9] D. B. Kunkee and A. J. Gasiewski, "Simulation of passive microwave wind direction signatures over the ocean using an asymmetric-wave geometrical optics model," *Radio Sci.*, vol. 32, p. 59, 1997.

[10] V. G. Irisov, "Small-slope expansion for thermal and reflected radiation from a rough surface," *Waves Random Media*, vol. 7, pp. 1–10, 1997.

[11] J. T. Johnson, R. T. Shin, L. Tsang, K. Pak, and J. A. Kong, "A numerical study of ocean polarimetric thermal emission," *IEEE Trans. Geosci. Remote Sensing*, vol. 37, pp. 8–20, Jan. 1999.

[12] A. G. Voronovich, *Wave Scattering From Rough Surfaces*. Berlin: Springer-Verlag, 1994.

[13] M. Zhang and J. T. Johnson, "Theoretical studies of ocean polarimetric brightness signatures," in *Proc. IGARSS'98*, vol. 5, 1998, pp. 2333–2335.

[14] Y. Cai and J. T. Johnson, "Theoretical study of ocean up/down wind brightness temperature differences with the small slope approximation," in *Proc. IGARSS'00*, Hamburg, Germany, 2000.

[15] J. T. Johnson and M. Zhang, "Theoretical study of the small slope approximation for ocean polarimetric thermal emission," *IEEE Trans. Geosci. Remote Sensing*, vol. 37, pp. 2305–2316, July 1999.

[16] M. Zhang and J. T. Johnson, "Comparison of modeled and measured second azimuthal harmonics of ocean surface brightness temperatures," *IEEE Trans. Geosci. Remote Sensing*, vol. 39, pp. 448–452, Mar. 2001.

[17] S. H. Yueh, W. J. Wilson, S. J. Dinardo, and F. K. Li, "Polarimetric microwave brightness signatures of ocean wind directions," *IEEE Trans. Geosci. Remote Sensing*, pp. 949–959, Jan. 1999.

[18] V. G. Irisov, "Azimuthal variations of the microwave radiation from a slightly non-Gaussian sea surface," *Radio Sci.*, vol. 53, pp. 65–82, 2000.

[19] J. T. Johnson, "Third order small perturbation method for scattering from dielectric rough surfaces," *J. Opt. Soc. Amer. A*, vol. 16, pp. 2720–2736, 1999.

[20] ——, "Erratum: Third order small perturbation method for scattering from dielectric rough surfaces," *J. Opt. Soc. Amer. A*, vol. 17, p. 1685, 2000.

[21] S. Elgar and R. T. Guza, "Observations of bispectra of shoaling surface gravity waves," *J. Fluid Mech.*, vol. 161, pp. 425–448, 1985.

[22] L. Tsang, J. A. Kong, and R. T. Shin, *Theory of Microwave Remote Sensing*. New York: Wiley, 1985.

[23] S. H. Yueh, R. Kwok, and S. V. Nghiem, "Polarimetric scattering and emission properties of targets with reflection symmetry," *Radio Sci.*, vol. 29, pp. 1409–1420, 1994.

[24] A. K. Fung, *Microwave Scattering and Emission Models and Their Applications*. Norwood, MA: Artech House, 1994.

[25] K. S. Chen and A. K. Fung, "A Bragg scattering model for the sea surface," in *Proc. Ocean'90 Conf.*, 1990, pp. 249–252.

[26] S. Elgar, "Relationships involving third moments and bispectra of a harmonic process," *IEEE Trans. Acoust., Speech, Signal Processing*, vol. ASSP–35, pp. 1725–1726, 1987.

[27] J. T. Johnson, "Comparison of the physical optics and small slope theories for polarimetric thermal emission from the sea surface," *IEEE Trans. Geosci. Remote Sensing*, to be published.

[28] L. A. Klein and C. T. Swift, "An improved model for the dielectric constant of sea water at microwave frequencies," *IEEE Trans. Antennas Propagat.*, vol. AP-25, pp. 104–111, 1977.

[29] C. Cox and W. Munk, "Measurement of the roughness of the sea surface from photographs of the sun's glitter," *J. Opt. Soc. Amer.*, vol. 44, pp. 838–850, 1954.

[30] M. S. Longuet-Higgins, "On the skewness of sea surface slopes," *J. Phys. Oceanogr.*, vol. 12, pp. 1283–1291, 1982.

[31] J. R. Apel, "An improved model of the ocean surface wave vector spectrum and its effects on radar backscatter," *J. Geophys. Res.*, vol. 99, pp. 16 269–16 291, 1994.

[32] S. L. Durden and J. F. Vesecky, "A physical radar cross-section model for a wind driven sea with swell," *IEEE J. Oceanic Eng.*, vol. OE-10, pp. 445–451, 1985.

[33] T. Elfouhaily, B. Chapron, K. Katsaros, and D. Vandemark, "A unified directional spectrum for long and short wind-driven waves," *J. Geophys. Res.*, vol. 102, pp. 15 780–15 796, 1997.

[34] V. S. Etkin, N. N. Vorsin, Yu. A. Kravtsov, V. G. Mirovskii, V. V. Nikitin, A. E. Popov, and I. A. Troitskii, "Critical phenomena with the thermal radio irradiation of a periodically uneven water surface," *Izvestiya: Radiophys. Quantum Electron.*, vol. 21, pp. 316–318, 1978.

[35] E. Elfouhaily, D. R. Thompson, D. Vandemark, and B. Chapron, "Higher-order hydrodynamic modulation: Theory and applications for ocean waves," *R. Soc. London A*, 2000, submitted for publication.

[36] T. Hara and W. J. Plant, "Hydrodynamic modulation of short wind-wave spectra by long waves and its measurement using microwave backscatter," *J. Geophys. Res.*, vol. 99, pp. 9767–9784, 1994.

[37] J. T. Johnson, J. V. Toporkov, and G. S. Brown, "A numerical study of backscattering from time evolving sea surfaces: Comparison of hydrodynamic models," *IEEE Trans. Geosci. Remote Sensing*, to be published.

[38] V. Chandran and S. Elgar, "Bispectral analysis of two-dimensional random processes," *IEEE Trans. Acoust., Speech, Signal Processing*, vol. 38, pp. 2181–2187, 1990.

[39] W. J. Plant, "A relationship between wind stress and wave slope," *J. Geophys. Res.*, vol. 87, pp. 1961–1967, 1982.

Joel T. Johnson (M'96) received the B.S.E.E. degree from the Georgia Institute of Technology, Atlanta, in 1991, and the S.M. and Ph.D. degrees from the Massachusetts Institute of Technology, Cambridge, in 1993 and 1996, respectively.

He is currently an Associate Professor in the Department of Electrical Engineering and ElectroScience Laboratory, The Ohio State University, Columbus. His research interests are in the areas of microwave remote sensing, propagation, and electromagnetic wave theory.

Dr. Johnson is an associate member of commissions B and F of the International Union of Radio Science (URSI), and a member of Tau Beta Pi, Eta Kappa Nu, and Phi Kappa Phi. He received the 1993 Best Paper Award from the IEEE Geoscience and Remote Sensing Society, and was named an Office of Naval Research Young Investigator, National Science Foundation Career Awardee, and PECASE Award recipient in 1997.

Yongyao Cai was born in Beijing, China, in 1974. He received the B.S. degree in electrical engineering from the Huazhong University of Science and Technology, Wuhan, China, in 1996. He received the M.S. degree in electrical engineering in 2000.

From 1998 to 2000, he was a Graduate Research Associate, ElectroScience Laboratory, The Ohio State University. He is currently an Electrical Engineer with Teradyne, Inc., Boston, MA.